

TOPICAL REVIEW • OPEN ACCESS

Path to the fabrication of efficient, stable and commercially viable large-area organic solar cells

To cite this article: Shafket Rasool *et al* 2023 *Mater. Futures* 2 032102



View the [article online](#) for updates and enhancements.

You may also like

- [Investigation of improvement in stability and power conversion efficiency of organic solar cells fabricated by incorporating carbon nanostructures in device architecture](#)
B V R S Subramanyam, Prakash Chandra Mahakul, Kadambinee Sa et al.
- [Revisiting open-circuit photovoltage decay in organic solar cells for the determination of bimolecular recombination constants](#)
Emi Nakatsuka, Kiyohito Mori, Naoki Ueno et al.
- [Simulating charge transport in organic semiconductors and devices: a review](#)
C Groves

Topical Review

Path to the fabrication of efficient, stable and commercially viable large-area organic solar cells

Shafket Rasool¹ , Jiwoo Yeop¹, Hye Won Cho¹, Woojin Lee¹, Jae Won Kim¹, Dohun Yuk¹ and Jin Young Kim^{1,2,*} 

¹ School of Energy and Chemical Engineering, Ulsan National Institute of Science and Technology, Ulsan 44919, Republic of Korea

² Graduate School of Carbon Neutrality, Ulsan National Institute of Science and Technology, Ulsan, 44919, Republic of Korea

E-mail: jykim@unist.ac.kr

Received 28 December 2022, revised 15 May 2023

Accepted for publication 16 May 2023

Published 16 June 2023



Abstract

Organic solar cells (OSCs) have reached an outstanding certified power conversion efficiency (PCE) of over 19% in single junction and 20% in tandem architecture design. Such high PCEs have emerged with outstanding Y-shaped Y6 non-fullerene acceptors (NFAs), together with PM6 electron donor polymers. PCEs are on the rise for small-area OSCs. However, large-area OSC sub-modules are still unable to achieve such high PCEs, and the highest certified PCE reported so far is ~12% having an area of 58 cm². To fabricate efficient large-area OSCs, new custom-designed NFAs for large-area systems are imminent along with improvements in the sub-module fabrication platforms. Moreover, the search for stable yet efficient OSCs is still in progress. In this review, progress in small-area OSCs is presented with reference to the advancement in the chemical structure of NFAs and donor polymers. Finally, the life-cycle assessment of OSCs is presented and the energy payback time of the efficient and stable OSCs is discussed and lastly, an outlook for the OSCs is given.

Keywords: organic solar cells, non-fullerene acceptors, OSC morphology, interfacial modification, light-soaking stability, solar energy, large-area OSCs

1. Introduction

Sunlight reaching Earth in 1 hour has more energy in it than the combined energies obtained from all the available energy (renewable and non-renewable) sources except solar.

* Author to whom any correspondence should be addressed.



Original content from this work may be used under the terms of the [Creative Commons Attribution 4.0 licence](https://creativecommons.org/licenses/by/4.0/). Any further distribution of this work must maintain attribution to the author(s) and the title of the work, journal citation and DOI.

Currently, most of the energy demand worldwide is being met via burning non-renewable fossil fuels that have drastic effects not only on human health but it also deteriorates the ecological environment, jeopardizes the sustainability of human life on planet Earth with the emission of greenhouse gases (GHGs), which contributes to global warming [1]. To offset these associated negative effects of energy from fossil fuels and to meet the ever-growing energy demand due to urbanization, industrialization, etc, we need to shift our energy dependence from fossil fuels towards inexhaustible and greener energy sources, such as solar energy, which has a minimum environmental footprint.

The idea of utilizing sunlight for energy purposes is not new and dates from 1954, when a team of scientists at Bell's lab invented the first silicon (Si) based solar cell with 6% efficiency. These inorganic solar cells were mostly used to power satellites [2]. Since then, a new era began with the utilization of a limitless source of energy from the Sun to fulfill human energy needs. Currently, the highest power conversion efficiency (PCE) of the amorphous Si and crystalline Si heterostructure-based solar cell has reached 26.3% [3]. Now, Si-solar cells possess more than 95% of the solar market share [4]. The history of organic solar cells (OSCs) starts with Tang, who reported 1% PCE for two-layered organic photovoltaic (OPV) cells in 1986 [5]. When the National Renewable Energy Laboratory started tabulating record PCEs of OSCs in 2001, 2% of the PCE was reported by scientists from the University of Linz [6]. OSCs got off to a slow start in terms of PCE, but over the past two decades, certified PCE of binary-component-based OSCs has reached 18.2% for single junction, while 20% has been achieved for tandem structure OSCs [7, 8]. Recently, the certified PCE of ternary single-junction OSCs has reached an unprecedented 19.2% [9]. This unprecedented improvement in the PCE of OSCs by an order of magnitude over the past two decades has re-invigorated this class of energy-harvesting devices and now, research from the commercialization aspects of OSCs is underway.

To put the scale of research on small-area OSCs and large-area OSC sub-modules into perspective, Jorgensen carried out a meta-analysis of ~9000 published research articles until 2012 and found out that >85% of the OSCs fabricated have an area of $\leq 0.2 \text{ cm}^2$ [10]. The best-performing small-area OSC showed an outstanding PCE of >13% in 2017 [11], while the OSC sub-module's PCE still stood at 7.189% for an area of over 70 cm^2 [12]. PCEs of the large-area OSC sub-modules are much lower than small-area champion cells due to multiple issues, including morphological issues between photoactive electron donor and acceptor materials, and packing features when these materials are slot-die or blade-coated in air (will be discussed in further detail in the following section). However, the advent of Y6-shaped non-fullerene acceptors (NFAs) has changed the landscape altogether and started pushing PCEs of NFA-based OSC sub-modules of over 12% having an area of over 50 cm^2 [13].

In this review, we have focus on how PCEs of small-area OSCs have evolved over time to reach this milestone with respect to NFA design, large-area OSC sub-module fabrication, and light-soaking (LS) stability of OSCs. From the commercialization aspect, the morphological aspects of small-area OSCs are discussed and compared with the large-area OSC sub-module morphology, so that similar performances on the large-area sub-module scale can be obtained. Finally, the life-cycle assessment (LCA) of OSCs is concisely discussed along with a brief outlook for OSCs.

2. Small-area single-junction and tandem OSCs

The development of various donor polymers and acceptor small molecules has contributed to the efficiency improvement

of OSCs. Before mainstream research and breakthrough PCEs in NFA-based OSCs, research mainly focused on controlling the crystallinity of the polymer as well as small-molecule electron donor components, while fullerenes including [6,6]-Phenyl-C61-butyric acid methyl ester (PC₆₁BM), [6,6]-Phenyl-C71-butyric acid methyl ester (PC₇₁BM), indene-C60 bisadduct (ICBA), etc. were used as electron acceptors. Various approaches were employed, such as pre- and post-thermal annealing to induce a stronger fibril network between photoactive materials [14, 15], solvent vapor annealing to induce the crystallinity in the photoactive blend film [16, 17], the use of processing solvent additives to tune aggregation of the photoactive materials [18–20], the addition of a ternary component to binary blend film to complement absorption [21, 22], etc. However, with the introduction of highly aggregated donor polymers based on naphtha-thiadiazole (NT) and difluoro-benzothiadiazole (BT) polymer backbone core, PCEs of the fullerene-based binary component containing single-junction OSCs reached over 10% for the first time, with the highest PCE reaching 11.5% employing PffBT4T-C₉C₁₃ electron donor polymer (figures 1(a) and (b)), while later certified PCE of 11.67% was also reported using PNTz4T-1F electron donor polymer [23–26]. The underlying idea for these high PCEs was embedded in the fact that these polymers showed temperature-dependent aggregation (TDA) tendency, which was exploited to form pure domains of polymers that helped in efficient exciton dissociation at the donor–acceptor interface, leading to higher current densities, with external quantum efficiencies reaching over 80% in the visible region due to their molecular orientations in the face-on direction and relative higher domain purity (figures 1(c)–(e)). During the early to mid 2010s, research focused on exciton dissociation, charge separation, charge transfer, etc. within the photoactive layer, as well as the effective development of complete OSCs [27–30].

Since most of the fundamental research on OSCs was already carried out and fundamental routes and some techniques to improve PCEs were already well-established, the invention of the y-shape-like Y6 NFA, altogether re-invigorated the field of OSCs with an outstanding 15.7% PCE reported for the first time using Y6 NFA with PM6 donor polymer in conventional as well as inverted architectures [32]. Together with Y6 NFA, a series of polymers have also been synthesized to match well with NFAs to improve PCEs in OSCs, as shown in figure 2. PM6 is a wide bandgap copolymer with a backbone alternating electron-donating benzodithiophene (BDT) and electron-accepting fused-ring benzodithiophenedione (BDD) units. Yu *et al* reported D18 polymer with a similar electron-donor BDT core consisting of an electron-accepting dithienobenzothiadiazole (DTBT) unit in its backbone [33]. D18:Y6 binary blend showed a stronger fibril network and reported the first-ever binary component containing single-junction OSCs with the highest PCE of 18.22%. Employing wide-bandgap D18 polymer as a ternary component in the PM6:L8BO system, Zhu *et al* reported PM6:D18:L8BO ternary photoactive system-based OSC with PCE as high as 19.6% [9]. The reason for such high PCE is due to the formation of a double-fibril network that is found to be better for exciton dissociation and charge transport in OSCs.

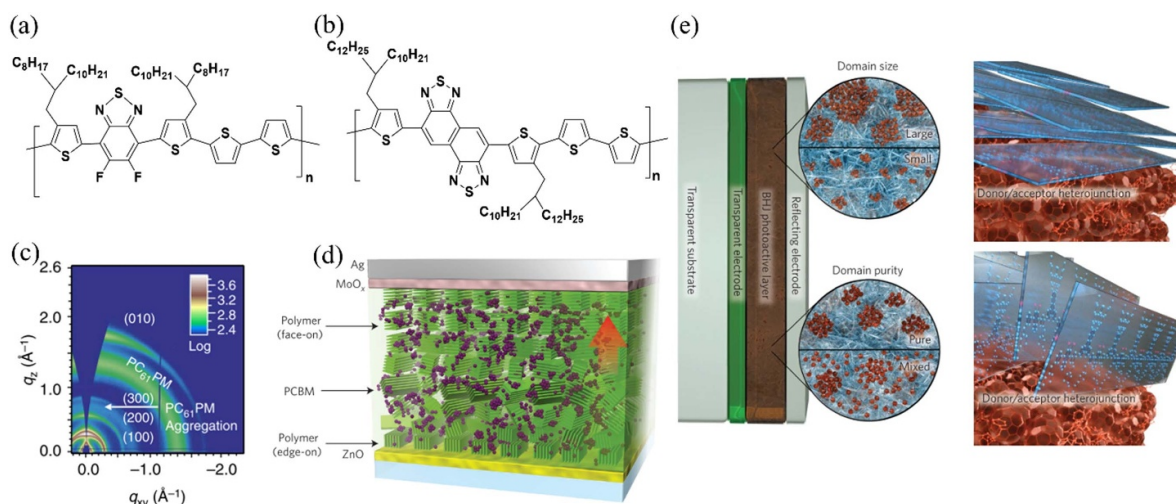


Figure 1. (a) Chemical structures of TDA type high-aggregation PffBT4T-2OD polymer [24], (b) PNTz4T [23] polymer. (c) 2D-GIWAXS image of PffBT4T-2OD:PC₆₁BM polymer. Reproduced from [24]. CC BY 4.0. (d) Schematic diagram of the efficient inverted OSCs based on PNTz4T:PCBM. Reproduced from [23], with permission from Springer Nature. (e) Schematics of the domain purity and molecular orientations in polymer:PCBM blend system. Reproduced from [31], with permission from Springer Nature.

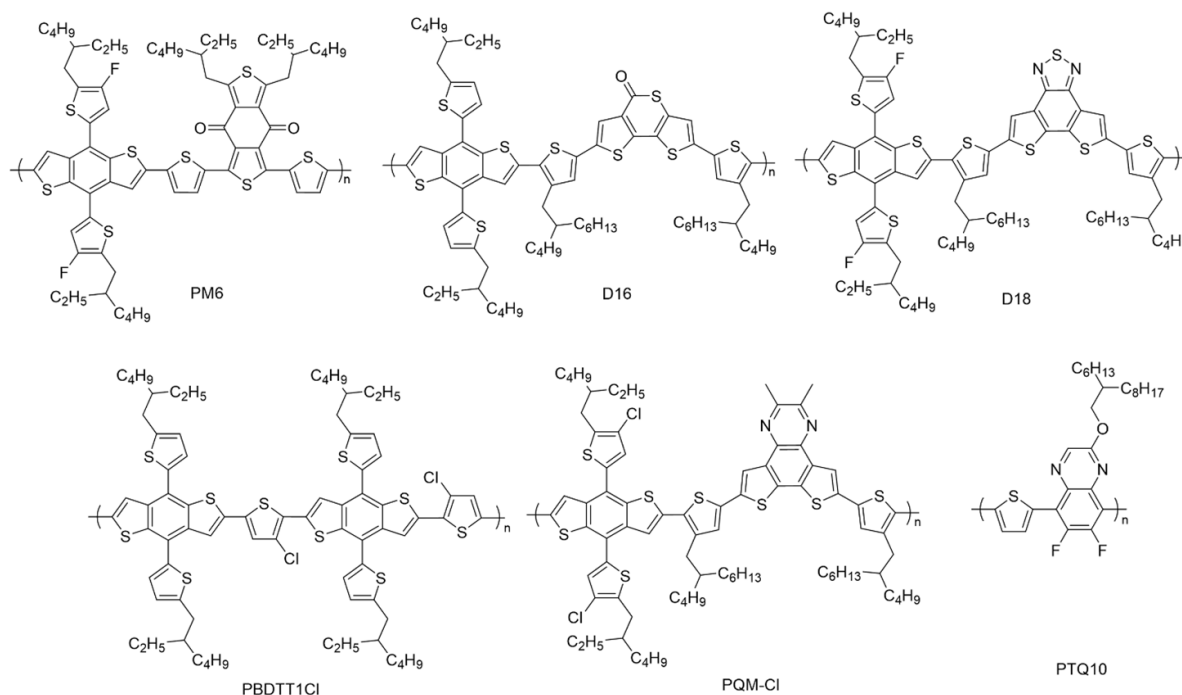


Figure 2. Chemical structures of the donor polymers for efficient OSCs [32, 34–37].

Wang *et al* designed and synthesized new wide-bandgap donor polymers with weak intramolecular charge transfer (ICT) effect, with different chlorine atoms in the thiophene connecting units of the polymer backbone and blended them with Y18-1F NFA [34]. These wide-bandgap-containing polymers, namely PBDTT, PBDTT1Cl and PBDTT2Cl, showed the lowest non-radiative energy loss of only 0.19 eV and resulted in 17.1% PCE.

In addition to donor polymers, most of the research in the pursuit of fabricating high-efficiency OSCs is being carried out to find suitable Y6 NFA derivatives for multiple purposes, such as better π - π stacking between NFA backbones

for efficient carrier transport, better light-harvesting in the near-infrared region, semi-transparent OPVs, etc. Yuan *et al* first reported Y6 NFA that employs a ladder-type electron-deficient-core-based central fused ring (dithienothiophen[3,2-b]-pyrrolobenzothiadiazole) with a benzothiadiazole (BT) core to fine-tune its absorption and electron affinity [32]. Unlike TDA polymer-based efficient OSCs where high processing temperature of solution and substrate was necessary, these Y6 NFA-based OSCs were processable at room temperature (RT) and showed good fibril network with appropriate phase separation between donor and Y6-NFA [32]. Based on this paper, studies have been actively conducted to

Table 1. PCEs of single-junction and tandem OSCs.

Photoactive system	Solvent	V_{OC} (V)	J_{SC} (mA.cm ⁻²)	FF (%)	PCE (%)	References
PM6:Y6 ^a	CF + CN	0.82	25.2	76.1	15.7	[32]
PM6:Y6-Se ^a	CF	0.82	25.47	75	15.82	[33]
PBDB-TF:BTP-4Cl ^a	CF + DIO	0.867	25.4	75.0	16.5	[40]
PM6:mBzS-4F ^a	CF + CN	0.804	27.72	76.35	17.02	[46]
PM6:Y6hu ^a	o-Xyl	0.87	25.6	77.9	17.4	[39]
PTQ10:m-BTP-C6Ph ^a	CF + CN	0.883	25.3	79.3	17.7	[42]
PTQ10:BTP-Ph ^a	CF + CN	0.888	24.7	77.9	17.1	[47]
PTQ10:BTP-Ph:BTP-Th ^a	CF + CN	0.888	25.2	78.6	17.6	[47]
PM6:Y6:BTO:PC71BM ^a	p-Xyl	0.85	27.12	75.75	17.41	[48]
PM6:L8-BO ^a	CF + DIO	0.888	25.7	79.9	18.2	[9]
D18:Y6 ^a	CF	0.859	27.70	76.6	18.22	[35]
PM6:L8-BO ^a	CF + DIO	0.87	25.72	81.5	18.32	[38]
PM6:BTP-eC9:BTP-F ^a	—	0.858	26.99	79.7	18.45	[49]
PM6:BO-4Cl:BO-5Cl ^a	CF + DIO	0.874	26.93	78.8	18.56	[8]
PM6:PM7-Si:BTP-eC9 ^a	CF + DIO	0.866	27.18	80.1	18.9	[50]
PM6:D18:L8-BO ^a	CF + CN	0.896	26.7	81.9	19.6	[9]
PM6:AITC/PM6:AITC:BTP-eC9 ^b	CB + DIO	1.92	13.6	74.6	19.4	[51]
	CF + DIO					
PBDB-TF:ITCC/PBDB-TF:BTP-eC9 ^b	CF + DIO	1.910	14.21	72.37	19.64	[44]
PBDB-TF:GS-ISO/PBDB-TF:BTP-eC9 ^b	Xyl + DIO	2.01	13.14	76.75	20.27	[7]
	CF + DIO					

^a Single-junction OSCs.^b Tandem OSCs.

Structurally, the tandem devices consist of a front cell absorbing a short wavelength region, a back cell absorbing a long wavelength region, and an interconnecting layer (ICL) to connect these layers [43, 44]. The front and the back cells usually consist of complementary absorption wavelengths to match their spectral response to the overall incident light, provided that the ICL has excellent optical and electrical properties to output the maximum PCE from the solar cell [7]. Liu *et al* modified the ICL using ZnO NPs:PEI/PEI/PEDOT:PSS (poly(3,4-ethylenedioxythiophene) polystyrene sulfonate) as the ICL, tuned the current obtained from the front sub-cell to effectively utilize incident photon, and matched the current generated in a front sub-cell with the rear sub-cell, finally resulting in a PCE of 18.71% (certified PCE of 18.09%) [43]. Using a similar strategy for optimizing the current generation in front and rear sub-cells by varying the sub-cell D:A composition and thickness, Wang *et al* fabricated efficient tandem OSCs reaching an outstanding PCE of 19.64% (certified PCE of 19.50%) [44]. For tandem OSCs, current matching between the front and the rear sub-cells not only plays a big role in the total output J_{SC} from the tandem device, but it also helps in achieving a higher FF; a factor that is strongly dependent on the balance of the charge carrier generation in both cells as well as the quality of the ICL. Zheng *et al* developed an electron-beam-evaporated TiO_x with PEDOT:PSS as the ICL, which results in not only efficient charge carrier extraction, but also has a low Schottky barrier for efficient charge recombination at the ICL interface [7]. As a result, Zhang *et al* was able to fabricate the highest ever PCE from an OSC with a PCE of 20.2% (certified PCE of 20%), due to the outstanding ICL (table 1).

3. Large-area OSCs

Although PCEs on small-area cell-scale have reached unprecedented values of over 19% for single-junction and >20% for tandem OSCs, PCEs on large-area-scale still lag their small-area counterparts. PCEs of the few representative large area OSCs having an area of >20 cm², is tabulated in table 2. For polymer:PCBM photoactive systems, one of the issues for low PCE for large-area OSC sub-modules lies in the un-optimized morphology due to the high aggregation tendency of the donor polymer. Rasool *et al* reported that when a highly aggregated PNTz4T polymer is processed (using PC₇₁BM as the acceptor) at RT, highly aggregated domains of the donor polymer are formed, which seriously limits the exciton dissociation and charge collection (figure 4(B)) [52]. They modified PNTz4T polymer with an MTC unit to fabricate PNTz4T-5MTC copolymer that was fully processable at RT, and fabricated a large-area OSC sub-module that resulted in 6.61% PCE on 54.45 cm² from the halogen-free solvent system, in comparison to the 4.29% for PNTz4T:PC₇₁BM blend film (figure 4) [52]. For a well-known PM6:Y6 photoactive system, Zhang *et al* introduced the concept of the reversible and sequential layer-by-layer (RS-LBL) method, in which the non-uniformity of the underlying PM6 polymer layer is solved by coating the second layer of PM6 over already coated PM6, but in the opposite direction, followed by Y6 NFA coating [53]. This method results in the uniform coating of the photoactive film resulting in reduced recombination losses. Thus, an OSC sub-module with 13.47% PCE has been reported in an active area of 36 cm² [53]. The use of an ethylene glycol chain containing NFA can also render

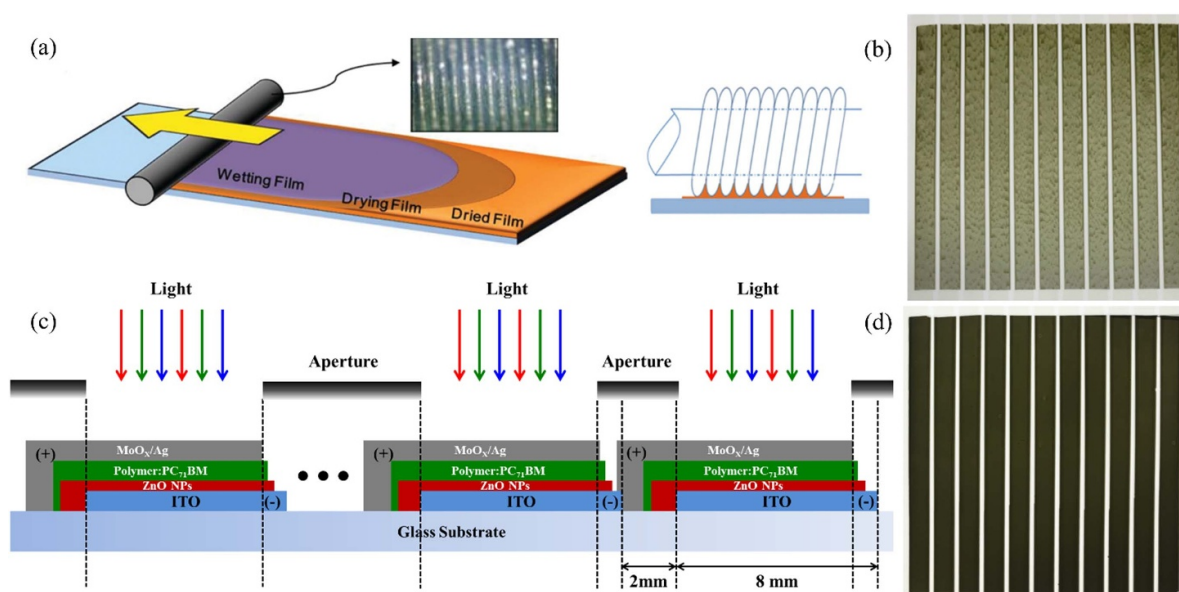


Figure 4. (a) Film-forming process via bar-coating. [60] John Wiley & Sons. [Copyright © 2013 WILEY-VCH Verlag GmbH & Co. KGaA, Weinheim]. (b) Bar-coated film of PNTz4T:PC₇₁BM. (d) Bar-coated film of PNTz4T-5MTC:PC₇₁BM blend film. (c) Schematics of the complete OSC sub-module. [52] John Wiley & Sons. [© 2019 WILEY-VCH Verlag GmbH & Co. KGaA, Weinheim].

Table 2. PCEs of large-area OSCs with area ≥ 20 cm².

Photoactive system	Coating method	Area (cm ²)	V_{oc} (V)	J_{sc} (mA.cm ⁻²)	FF (%)	PCE (%)	References
TPD-3F:IT-4F	Blade-coating	20.4	4.52	3.50	64	10.13	[67]
PM6:Y6	Blade-coating	36	9.04	1.63	49.42	7.31	[48]
PM6:Y6:BTO:PC ₇₁ BM	Blade-coating	36	10.02	2.01	70.8	14.26	[48]
PNTz4T-5MTC:PCBM	Bar-coating	54.45	7.97	1.3406	61	6.61	[52]
PTB7-Th:T2-OEHRH	Bar-coating	55.5	11.47	1.29	63	9.32	[68]
PBDB-T:CNDTBT-C8IDT-FINCN	Bar-coating	54.45	8.16	1.68	67.2	9.21	[69]
PBDB-TF:IT-4F	Blade-coating	58.5	8.80	1.71	60	9.03	[70]
PBDB-T-2F:N3:P(NDI2OD-T2)	Blade-coating	20.61	6.96	2.94	69.88	14.31	[66]
	Blade-coating	58.5	8.61	2.43	67.10	14.04	[66]

an ordered microstructure into the photoactive film, leading to an efficient annealing-free large-area OSC sub-module [48]. Cho *et al* synthesized a Y6-derivative with CF₃-terminated side-chain and obtained 16.1% PCE in an area of 1 cm² [54].

For the fabrication of large-area OSC sub-modules, various methods have been reported in the literature, which range from spin-coating 10 cm × 10 cm area substrates [55], bar-coating [52], blade-coating [56, 57], slot-die coating [58], etc. The bar-coating process involves three main steps: (1) wetting of the bar via dropping the solution onto the bar, (2) wet coating of the polymer solution by the horizontal movement of the coating bar relative to the substrate and (3) drying of the wet film (figure 4(a)). The groove of coils on the wire bar (D-bar) determines the amount of blend solution as it moves along the substrate. Thickness, roughness and uniformity of the film are determined by various experimental factors, such as the viscosity, surface tension of the solvent, the surface energy of the substrate, the speed of the coating bar, and the distance between the substrate and the coating bar. Blade-coating is a similar method as compared to bar-coating,

with the difference that it uses the blade instead of the bar. In addition, the organic solution is loaded directly onto the coating bar in the bar-coating process, whereas the solution is loaded onto the substrate in the blade-coating process [59, 60]. Both methods are very well suited to the coating of thin photoactive films using a small amount of the solution. One of the issues related to the reduced PCE of the large-area OSC sub-modules is maintaining the morphology of the photoactive film when coated via blade-coating, slot-die coating, or bar-coating methods. This is an important factor as the drying process during the solidification of the photoactive film is very different from the robust spin-coated drying method where optimized morphology is usually obtained in small-area OSCs. This is why the upscaling method for the solution-processed OSCs is relatively challenging at the moment but could be better understood with further investigations in the future.

Traditionally, spin-coated sub-modules obtained higher PCEs in comparison to tedious slot-die coating methods. For instance, Sachin *et al* reported a series of 2D-BDT-based polymer donors with various numbers of BDT units and

examined how the number of BDT units influences the interconnectivity in the bulk-heterojunction (BHJ) [55]. In BDT₂, two BDT units induced strong intermolecular interactions, enhancing exciton diffusion and free-charge-carrier transport. A spin-coated sub-module employing BDT₂:PC₇₁BM blend resulted in 7.45% PCE in a 77.8 cm² area. This enhanced PCE is attributed to reduced charge recombination and a well-constructed 3D morphology. Moon *et al* developed solution-processable hybrid hole transport layers (h-HTLs) incorporating WO₃ and MoO₃ [61]. With easily controllable energy levels due to the high electronegativity of W and Mo atoms, h-HTLs showed well-matched energy levels for both deep and low-lying highest occupied molecular orbital energy levels of the photoactive materials. Lim's group first reported dopamine hydrochloride (DA) molecular linker as an organic interfacial layer for interfacial engineering of ZnO electron transport layer (ETL) [62]. Due to the strong electron donation of DA, the localized orbitals of surface-bound ligands were coupled with the delocalized conduction band of ZnO, improving charge transfer at the ZnO/photoactive layer interface. In addition, the work function (WF) of pristine ZnO was reduced from 4.7 to 4.3 eV, which induced favorable energy-level alignment between the ETL and the photoactive layer. Consequently, a semi-transparent flexible sub-module with PTB7:PC₇₁BM photoactive layer using the spin-coating method achieved 6.43% of PCE having 41.45% transmittance at 550 nm, having an area of 40 cm². The same group then developed a cross-linkable new polyelectrolyte ETL (c-PEIE) based on cobalt(II) ion doping to polyethyleneimine ethoxylated (PEIE) [63]. The cross-linking behavior removed lone-pair electrons from amine groups in PEIE, suppressing the reaction with NFAs, while low WF c-PEIE ETL was achieved in their work. PM6:Y6:PC₇₁BM blend films containing sub-modules fabricated via spin-coating resulted in an excellent PCE of 13.12% for a 50 cm² area and 7.41% for a 300 cm² photovoltaic panel. Recently, Chin *et al* presented a flexible low-WF transparent composite electrode, Ag grid/silver nanowires (AgNWs):zinc-chelated polyethyleneimine (PEI-Zn) [13]. AgNWs:PEI-Zn was deposited on Ag grid to facilitate electron collection with high transmittance, high conductivity, low surface roughness, low WF, good mechanical properties and good thermal stability due to the electrostatic interaction between PEI-Zn and AgNWs. Using a spin-coated PM6:Y6:PC₇₁BM photoactive layer, they obtained a high-performance flexible large-area module with PCE of 13.2% for 54 cm² of the active area.

Spin-coating is a material consumptive method in which a nearly 1.5 ml solution of the photoactive materials is required to fabricate a 10 cm × 10 cm sub-module, provided that the solution has very good wettability. On the other hand, with the same 1.5 ml volume, nearly ten such sub-modules of 10 cm × 10 cm size can be fabricated. For the practical applicability of OSCs, numerous coating methods are available and have been tested, such as screen printing, gravure printing, etc. However, slot-die or bar/blade-coating methods are most commonly employed to fabricate efficient OSC sub-modules because they are not only efficient from the material consumption perspective, but these methods more closely relate to the industrial roll-to-roll printing techniques, for which their integration is rather

easy [64]. In addition to their ease of processability via the abovementioned large-area coating methods, large-area OSC sub-module PCEs still lag behind the small-area PCEs. To date, PCEs of OSC sub-modules currently stand at ~14% for area <30 cm² for binary-component containing NFA-based OSCs fabricated via blade-coating [48, 65], while ternary and quaternary OSC sub-modules have reached PCE >14% with >30 cm² area [66]. Among various reasons for low PCE in OSC sub-modules (which is usually 80% of their best PCE in small-area OSCs), one of the fundamental reasons lies in the thickness intolerance of the photoactive systems. For instance, the first report of the Y6-NFA-based efficient OSC showed an optimum PCE of 15.7% at 100 nm thickness with 74.8% FF, while the same system showed a PCE of 13.6% with 62.3% FF at 300 nm thickness [32]. Imbalanced charge carrier mobility and enhanced recombination are prime reasons for such a drastic drop in PCE. Moreover, the reason for low PCE in blade-coated or bar-coated OSC sub-modules is partly due to the increased sheet resistance of the indium doped tin oxide (ITO) substrate with increasing area, and partly because it relates to the controlled morphology of the blend film on a large scale, thus limiting the maximum current output from the single stripe, which seriously limits the PCE when multiple stripes are attached in series.

Zhang *et al* controlled the crystallinity of the IT-4F NFA by increasing the heating temperature of the substrate during blade-coating [71]. At 30 °C heating of the substrate, IT-4F showed lower crystallinity. When Zhang *et al* increased the substrate temperature during blade-coating, not only the crystallinity of the IT-4F was enhanced, as witnessed in GIWAXS analysis, but also the long-range ordered side-chain packing was observed, also in GIWAXS, along with small-scale phase separation. This resulted in 11.39% PCE in a 0.56 cm² area. Liao *et al* synthesized the TPD-3F donor polymer specifically for large-area OSC sub-module applications and blended it with IT-4F [67]. The alkyl chain in TPB-3F improved the solubility of the donor and contributed to the interlamellar distance improvement, and showed a preferential out-of-plane packing feature in the final blend film, which resulted in a certified PCE of 10.1% in a 20.4 cm² area. Park *et al* enhanced the crystallinity of the ITIC NFA in the blend film with PM6 via accelerating the drying of the solvent with heating to 50 °C [67]. As a result, 9.03% efficient OSC sub-module was fabricated in an area of 58.5 cm². Sun *et al* introduced the LBL film formation process in the molecular ordering and crystallite sizes of the Y6-NFA were enhanced compared to the BHJ approach [72]. The LBL films showed high charge transport and charge extraction properties as well, thereby, resulting in 11.86% PCE for PM6/Y6 bilayer OSC sub-module achieved in the area of 11.52 cm², whereas the BHJ OSC sub-module showed 10.15% PCE under similar conditions.

Recently, Yoon *et al* fabricated the most efficient large-area OSC sub-module via the blade-coating method, by optimizing blend morphology via the addition of P(NDI2OD-T2) as a ternary component in PBDB-T-2F:N3 blend film [66]. The resulting OSC sub-module formed intricate charge carrier channels within the blend film, which proved effective for efficient exciton dissociation, balanced charge transport and reduced

recombination within photoactive films. This resulted in an OSC sub-module as efficient as 14.04% with a photoactive area of 58.5 cm², which is the highest PCE reported to date. In another attempt to fabricate efficient OSCs via blade-coating, Gong *et al* established the correlation between the chemical structures of the NFAs in the blend film and the processing solvent [73]. According to their results, excessive aggregations of the NFA exist due to the smaller side-chain present in the central pyrrole unit of the Y6–10 NFA. This steric hindrance can be avoided with larger alkyl chains, such as in BTP-eC9. Therefore, an OSC sub-module as efficient as 14.07% was fabricated in the area of 25.21 cm². To tune the morphology of the blend film, the use of the third component in the binary blend film has also proved to be effective. Chen *et al* synthesized an ethylene glycol side-chain containing a Y6-derivative called BTO [48]. The binary component-based OSC sub-module showed only 7.31% PCE due to excessive aggregation of the Y6-NFA in the blend film, which was regulated after the addition of the guest BTO in the blend system, and a quaternary OSC sub-module consisting of a PM6:Y6:BTO:PC₇₁BM photoactive system resulted in 14.26% PCE in the photoactive area of 36 cm². Interestingly, Chaturvedi *et al* coated a PEDOT:PSS HTL, a photoactive layer consisting of PTB7-Th:IEICO-4F and a ZnO ETL via slot-die coating and achieved an outstanding PCE of 11% [58].

In the above-mentioned OSC sub-modules, rigid substrates consisting of glass/ITO have been utilized, and solution-processed and thermally evaporated robust metal oxides have been used as charge transport channels, while much of the focus in the above-mentioned research is on optimizing the morphology of the photoactive blend system. Recently, researchers have tried to find alternatives to rigid glass substrates to fabricate efficient flexible OSCs. Zeng *et al* utilized a flexible transparent electrode comprising an ionic liquid with chloride ions and a dihydroxyl group to control the reduction of Ag in AgNW and at the same time, to form a better contact between reduced Ag and AgNW [74]. Employing this substrate, Zeng *et al* reported 17.5% PCE on the flexible substrate in the area of 0.06 cm², while 15.82% PCE was achieved with 1 cm² area flexible OSCs. Chen *et al* used a ‘welding’ approach to bind the upper electrode with the underlying polyethylene terephthalate (PET)-modified AgNWs to address transmittance as well as electrode binding issues of the flexible substrate. First, they modified the PET substrate with AgNWs, followed by the coating of Al-doped ZnO containing AgNWs to grow a AgNW-embedded network with low contact resistance and high adhesion to the substrate. As a result, a flexible transparent electrode (FTE) with 35.2 Ω·sq⁻¹ sheet resistance and >90% transmittance (excluding PET substrate) was fabricated, which showed 15.21% PCE in small-area OSCs [75]. In another work, Chen *et al* further introduced the ‘reinforced concrete’ strategy by adding polydopamine, which reduces Ag⁺ ions to form Ag-nanoparticles (AgNPs) and resulted in a AgNW:PDA:AgNP FTE, which showed a very high efficiency of 17.07% for flexible OSCs, but more importantly, these flexible OSCs maintained >80% of their initial PCE after 10 000 bending cycles [76]. A search for alternative electrodes to be used on flexible substrates is underway, but the

PCEs lag behind compared to the robust glass/ITO substrates due to sheet resistance of the flexible substrate as well as the difficulty in forming a uniform photoactive film on large-scale flexible substrates.

4. Morphological features of small to large-area OSCs

Ideally, the morphology of small area OSCs should also be reproduced on large-scale OSC sub-modules, but due to solution processability, it is a challenge to reproduce similar morphologies on a large scale. Pokuri *et al* compared the morphologies of the spin-coated P3HT/fullerene BHJ films with blade-coated films and found that the spin-coated and then annealed samples had better connectivity and uniformity throughout the blend film [77]. These spin-annealed films have larger domain sizes, which aids in exciton generation and dissociation, compared to blade-annealed photoactive films (figure 5(A)) [77]. On the other hand, blade-coated films lack this connectivity due to relatively less pure donor polymer phases, thereby limiting the charge transport channels. Dong *et al* studied an efficient PM6:Y6 system and found that due to excessive aggregation of the Y6 NFA, larger domains appeared limiting the hole-transfer efficiency from Y6 to PM6 [57]. By increasing the size of the alkyl chains in the central pyrrole unit of the Y6-NFA, morphologies in blade-coated films can be effectively controlled and reproduced via the blade-coating method as well. Li *et al* introduced a meniscus-guided coating approach to regulate the shear impulse during film formation and fabricated 15.50% PCE on the 1 cm² scale OSC [78]. Zhao *et al* controlled the aggregation and kinetics of the solution and film states using a hot slot-die coating process, which resulted in a PCE of 13.7% for o-Xyl and 13.8% for TMB-based OSCs in the area of 0.56 cm² [79]. Weng *et al* introduced a two-step sequential deposition (SD) technique to control the photoactive blend film’s morphology [80]. Using this approach, robust morphology of the SD blend film was formed with similar phase separation as spin-coated films, and resulted in higher PCE for SD OSCs than spin-coated OSCs. Liu *et al* also introduced a similar strategy called pseudo-planar heterojunction (PPH) and coated donor and acceptor films in two steps [81]. PM6 was blade-coated as the first layer, followed by IT-4F with indene-C60 bisadduct to regulate vertical phase separation. Following the PPH approach, PM6 accumulated underneath, while IT-4F was enriched at the surface while enhancing the crystallinity of the PM6 donor polymer. They were able to fabricate 14.25% PCE of PPH-coated OSCs compared to BHJ OSC with PCE of 13.73% in the area of 1.05 cm². Jee *et al* proposed that vertical phase separation and the crystallinity in individual photoactive layers (materials, such as donor polymer and NFA) can be effectively controlled using a sequential LBL approach (figure 5(B)) [82]. Using this approach, the morphology of the individual layer can be controlled via solvent additive and thermal annealing of the individual films, thus effectively reducing the geminate and non-geminate recombination losses. Therefore, it can

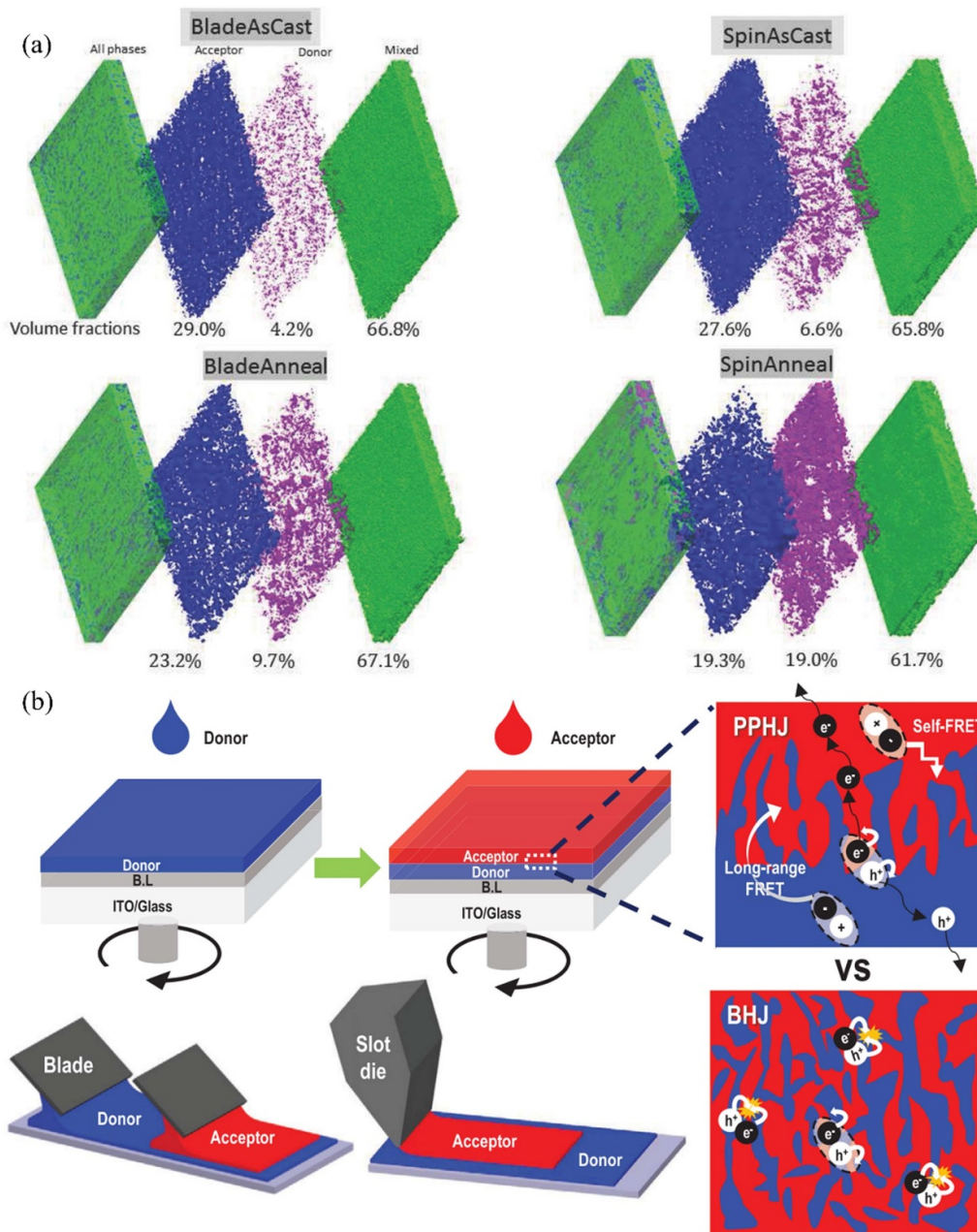


Figure 5. (a) Morphologies and volume-fractions of the photoactive materials processed via different coating methods. [77] John Wiley & Sons. [© 2017 WILEY-VCH Verlag GmbH & Co. KGaA, Weinheim]. (b) Sequential LBL-coated photoactive films and their proposed morphological evolution. Reproduced from [82]. CC BY 4.0.

be concluded that the morphology of the bar-coated or slot-die-coated films differ from spin-coated films, which limits the overall PCE of the BC films. Thus controlling and even improving the morphology of the blade/bar/slot-die-coated films is the key to enhance PCE of the air-processed OSCs.

5. Stability of OSCs

One of the key limiting elements for the commercialization of OSC sub-modules is their limited long-term operational LS stability under light and heat/humid conditions. Since small-area OSCs have already reached the benchmark 20% PCE, while OSC sub-modules reached >14%, the next

phase of OSC immense research is focused on their stability. There has been a gigantic number of reports related to the stability of the OSCs, but most of these researches have their own stability reporting procedure, which raises serious concern for the exact or uniform stability reporting procedure. Most of these reports have common external underlying factors, such as light, humidity, thermal stress, oxygen, moisture, etc. However, to standardize the stability qualification test, the international summit on OSCs established the consensus on OSC stability reporting procedures [83, 84]. The OSC community is now encouraged to report their stability results following the degradation category mentioned in these consensus statements.

Small area OSCs and the OSC sub-modules degrade due to multiple intrinsic factors (extrinsic factors as described above), which can be broadly categorized into three types: (1) intrinsically unstable photoactive materials under heat and/or light, (2) thermodynamically unstable nano-morphologies and (3) interfacial degradation [85]. To address the first category, intrinsically stable photoactive materials are the key to fabricating efficient and stable OSCs [85, 86].

Photo-degradation induced by incident light is divided into two mechanisms, namely photochemical and photophysical degradation. To suppress the photochemical degradation, mostly photo-oxidation, which occurs due to the permeation of oxygen and water into the photoactive layer, it is necessary to introduce encapsulating barriers and encapsulant with low oxygen transfer rate (OTR) and low water vapor transfer rate (WVTR) [87]. Angmo *et al* fabricated a 100 cm² ITO-free module with a compact encapsulation structure of barrier/adhesive/module/adhesive/barrier fastened with a button contact [88]. At low OTR (0.01 cm³ m⁻² d⁻¹ bar⁻¹) and WVTR (0.04 g m⁻² d⁻¹), T80, the duration over which a solar cell maintains 80% of its initial efficiency, is 2.22 years extrapolated from outdoor measurements. Hermosa *et al* studied the WVTR of transparent flexible ultra-high permeation barrier films (UHPBFs) [89]. They tested the WVTR via calcium tests and found that the application of an additional adhesion-promoting layer on a standard UHPBF reduces the WVTRs by a factor of 5.

Since photoactive films in OSCs consist of one electron donor and acceptor materials, these materials make pure and hybrid/mixed donor–acceptor interfaces throughout the bulk of the film to provide an exciton dissociation platform and charge transport channels for photogenerated carriers [90]. These donor–acceptor phases are not thermodynamically stable, and change over time once the OSCs are placed under continuous light shining towards thermodynamic equilibrium [91, 92]. Schaffer *et al*, using micro-focused GISAXS in which the incident beam is focused on the micrometer scale, showed that the nano-morphologies change over time causing a reduction in photocurrent. Earlier research into fullerene-based OSCs showed that the use of high-energy UV-photons causes the aggregation of PCBM, which can be avoided by using UV-cut filters when OSCs are subjected to LS tests [93, 94]. Liu *et al* showed that just putting a ≥ 400 nm UV-cut filter over OSCs during the LS test can circumvent these aggregations and lead to much enhanced LS stability compared to without a UV-cut filter-assisted LS test. Cheng *et al* introduced the simplest biphenol (BPO) chemical to be added into the blend film to assist molecular lock of the blend film [95]. BPO acts as a bridge between fluorine-atom-containing polymers and freezes the so-called nanomorphology to achieve higher LS stability in OSCs.

Wang *et al* reported that the use of the UV-crosslinkable π -conjugated polymer can lock the morphology of the blend film, and so the crystallization of PC₇₁BM acceptor can be reduced in fullerene-based OSCs [96]. Suppressing the aggregation and nanophase separation of blend film resulted in enhanced thermal as well as photostability of the fullerene-based OSCs.

Zhu *et al* used PC₇₁BM acceptor in a PTB7-Th:IEICO-4F photoactive system [97]. They suggested that if a third component has good miscibility with any component of the binary blend system (ca. PTB7-Th donor polymer), then, it can develop a more miscible phase with PTB7-Th donor polymer and can thus suppress the over-crystallization of IEICO-4F NFA, which occurs via the diffusion of the highly crystallizable IEICO-4F NFA out of the mixed phase [97]. In this way, controlling the over-crystallization of the acceptor phase from the thermodynamics aspect can help in achieving high stability in OSCs. Liu *et al* synthesized a multicomponent block copolymer PM6-b-L15 (namely S11) to altogether suppress the aggregation issues of the blend films over exposure to heat and light [98]. The resulting S11 multicomponent block copolymer-based OSCs maintain their fibril network, which is beneficial for exciton dissociation. For a blend film of PM6:L15, the appearance of the separated domains causes the reduction of the donor–acceptor interfacial area resulting in reduced exciton dissociation (figure 6). While in the case of S11 block copolymer a relatively fixed and dense morphology is formed. A small number of the PM6 or L15 polymers in the S11 block copolymer system can further fill any voids present in the blend film due to their interaction with the host S11 block copolymer, thus forming a compact morphology (figures 6(a) and (b)). In contrast to PM6:L15 blend film, the addition of the PM6 or L15 polymers into the S11 block copolymer system can effectively suppress the diffusion of the individual PM6 or L15 polymers (in the case of a binary component system of PM6:L15), and so a stable morphology can be obtained under thermal testing. The OSCs fabricated via this approach showed $\sim 80\%$ for S11 and $\sim 78.2\%$ for PM6-b-L15:PM6:L15, in comparison to 70.9% for the PM6:L15 photoactive system [98].

Introducing a more photo-stable interlayer is also a good strategy. Chang *et al* replaced ZnO, MoO₃ with PEI and PEDOT:PSS, respectively, to enhance the photostability [99]. The initial efficiency of the module with the architecture of ITO/PEI/PV2000:PCBM/PEDOT:PSS/Ag and the area of 23.7 cm² was 7.53%, then it maintained 91.7% of the initial value after the 1000 h LS test. In contrast, the module employing ETL/HTL as PEI/MoO₃ showed serious degradation and it failed after 144 h of light exposure. This suggests that PEDOT:PSS works as an effective interlayer to improve the photostability of the OPV module. Furthermore, Li *et al* employed a new organic molecule consisting of carboxylic acid at one end, whose function is to deactivate photoinduced catalysis of the ZnO, and called this new organic molecule as new modifying agent (NMA) [100]. Using D18:N3 as the active layer and adopting hybrid ZnO/NMA ETL to fabricate a 1 cm² area OSC could achieve 16.12% PCE. The operational stability under continuous 1 sun illumination under maximum power point tracking in a nitrogen-filled glove box was measured for small-area devices, then it maintained 95.4% of its initial PCE after 1500 h illumination, and T80 is extrapolated as 7572 h. It has remarkable photostability with high efficiency although it is performed in a small area. Dahlstrom *et al* introduced photoactive tri-azide cross-linkable material as an HTL

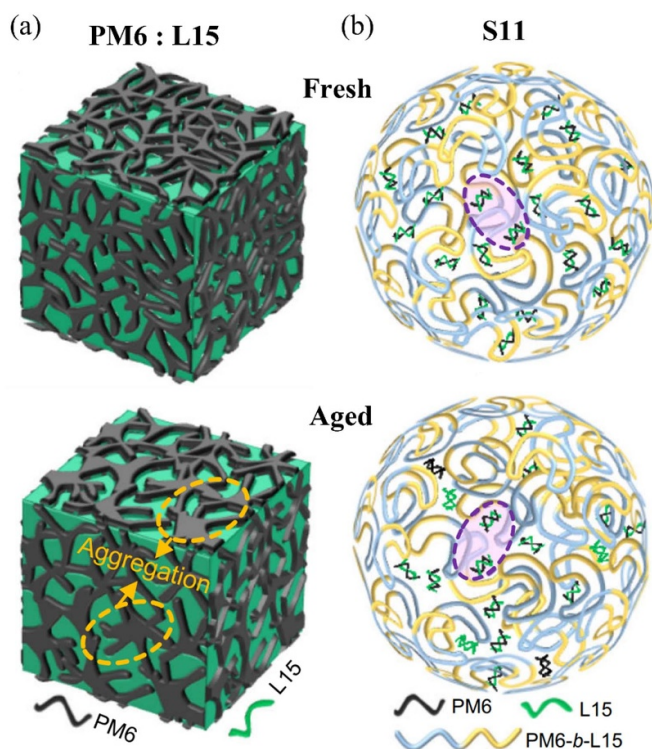


Figure 6. (a) Morphological evolution of the two-component blend film before and after the thermal ageing test. (b) Morphological evolution of single-component block-copolymer before and after the thermal ageing test. Reproduced from [98]. CC BY 4.0.

and found that the diffusion of the transport channel materials into the photoactive material is one of the major causes of the efficiency drop in OSCs [101].

Even though there have been numerous types of research related to LS stability of the OSCs, there is still a lack of studies on the light stability test of large-area modules over 100 cm² with high initial efficiency. Circumventing diffusion of oxygen and moisture into the photoactive materials, optimizing and even freezing the nano-morphologies of the blend films, improving the interfaces between charge transport layers and photoactive layers, etc, have all proved to be very beneficial but are mostly implemented in small-area OSCs. At the same time, fabricating light-soaked stable OSC sub-modules poses a whole new challenge to deal with since the large-area OSC sub-module could possess more defects and imperfect connections between active layers and interlayers. Further studies on the uniformity of film formation and their interactions with charge-transport layers at the large-scale would be required to fabricate a reliable OSC sub-module.

6. Life-cycle assessment of OSCs

Since GHG emissions are affecting almost every aspect of life needed to sustain life on planet Earth, much effort is being put into cutting or at least lowering GHG emissions. Therefore, the utilization of an inexhaustible and abundant source of energy, i.e. the Sun, is among the best possible solutions towards a greener and more sustainable future, but it does not warrant

that the new environmentally friendly solar energy technology does not emit any GHG into the environment during its production. One benchmark analysis to determine the feasibility of the energy technology in the market is LCA. For solar energy technologies, such as inorganic mono and crystalline Si, copper indium gallium selenide called as CIGS solar cells, etc, the LCA of these solar energies has been thoroughly carried out previously. However, for emerging solar energy technologies, such as OSCs and perovskite solar cells (PVSCs), LCA is not yet fully established. This does not imply that LCA has never been carried out for OSCs, but the underlying reason for not fully established LCA analyses is the improving PCEs, while still limiting LS stabilities of these emerging OSC and PVSC technologies, resulting in a change in already established parameters. For instance, the PCE of OSCs one decade ago was around 10%, and this PCE has nearly doubled over the past 10 years.

For LCA of solar energy technology, energy payback time (EPBT) and GHG emissions are the chief parameters to consider and are most discussed in the literature. EPBT is the time needed by the given technology to return the input energy to fabricate it [102]. While the construction of the solar energy panels has inbuilt CO₂ and few GHG emissions associated with them, CO₂ equivalent per kWh is the most compared parameter for GHG emissions between energy production technologies. To put this into perspective, silicon solar cells emit 22.1–38.1 g CO₂ equivalent per kWh [103], while this value stands at 5–7 g CO₂ equivalent per kWh for an efficient OSC sub-module with PCE of 10% while having a 20 year lifetime [104], implying the advantages of OSC technologies. In another comparison, the OSC has GHG emission at 78.99 g CO₂ equivalent per kWh [103]. On the other hand, depending on the type and location of the OSC technology, EPBT for cSi solar cells stands at around 1 year, while this value varies from 51 d to 1.1 years for OSCs [102, 105]. During 2020–2021, the levelized cost of electricity has reduced by 13% due to significant improvements in performance.

7. Future perspectives

PCEs of OSCs have already surpassed a psychological barrier of 20% for tandem-structured and over 19% for single-junction OSCs, mainly due to innovative material designs and device engineering approaches. To utilize OSCs for practical applications, such as flexible electronics, indoor photovoltaics, near infrared-photodetectors, etc, their PCEs not only need to be improved, but their LS stabilities also need considerable improvement. High PCEs and LS stabilities will ultimately lower the EPBT of the OSCs, which could push this class of energy-harvesting technology into the competitive solar energy market.

PCEs on large-area systems can improve with custom-designed electron donor polymers and NFAs that have better morphology along with suitable molecular packings when bar/blade/slot-die coated. For instance, the molecular design of the donor polymers, fullerene or NFAs plays a key role in terms of incident photon absorption, defining the

extent of exciton dissociation and charge transport within the photoactive blend film. Designing these materials is imminent, which will not only result in the formation of robust nano-morphologies with appropriate nano-phase separation and crystallinity leading to reduced recombination, but will also show high mobility so that relatively thicker photoactive films can also be fabricated, which is an important factor for the upscaling of OSCs. This can be achieved via the modified end-groups of photoactive materials for effective charge-transport via backbone, side-chain engineering to facilitate solubility, synthesis of block-copolymers to freeze or lock-in the nanomorphology, introduction of electronegative atoms (such as halogens) to synthesize materials with high dipole moments, design of NFAs or solid additives with reasonably higher quadrupole moments in the local nanomorphology of the blend film, modification of side-chains of the donor polymers or NFAs for enhanced face-on stacking and crystallinity of materials, etc.

In addition to material modification, an upgradation of the coating system is also needed. For instance, for speeding up the drying of the solvent to quickly solidify the photoactive film, one can introduce the N₂-gas purge over the coated film, which has been proven to be beneficial in recent reports [65]. Moreover, the use of solution-processable transport layers will also be needed to fabricate fully-solution processable OSCs, in place of currently used thermally evaporated (for instance, MoO₃ in the case of inverted OSCs) charge-transport buffer layers. Another important factor is the use of flexible substrates instead of glass/ITO substrates. Since one of the main advantages of OSCs is their flexibility, the use of alternative substrates, such as PET/ITO or PET/silver-nano-mesh type, is necessary. To form the uniform pinhole-free uniform film, innovative coating designs, such as LBL methods (such as RS-LBL), the use of ternary or quaternary photoactive systems, control of coating conditions to lower the coffee-ring effect (such as in bar-coated photoactive films), etc, will also be helpful. Most importantly, after the drying of the photoactive films the solvent will evaporate into the environment. Therefore, solvents will be required to have good solubility for the photoactive materials and minimum impact on the environment, and the quest for greener and halogen-free solvent systems is in progress.

To utilize OSCs for commercial applications, one of the most important criteria for their consideration is their stability under light, humidity and thermal conditions. Although photoactive materials with stable yet UV-resisting chemical structures can be effectively tuned via robust molecular modification, their morphological stability is the main area of interest for researchers working on their commercialization. To achieve higher morphological stability, cross-linkable photoactive materials are one way to tackle this issue. Although these cross-linkable materials might result in similar or slightly lower PCE than their un-crosslinked counterparts, their LS stability could be reasonably higher. Fixing the nanomorphology via the addition of cross-linkable (such as azide) materials into the photoactive blend film is another approach that has proved to be beneficial in this aspect. The use of single-component polymers is another approach to achieving

robust and photo-stable nanomorphology. The design of efficient charge-transport buffer layers also needs immediate attention, as the interface between organic photoactive films and metal oxides acts as starting point for either degradation or their efficiency of charge transport diminishes over the passage of time under light, heat and humid conditions.

After successfully addressing these issues and keeping in view the key requirements for the fabrication of efficient yet stable small-area and large-area OSC sub-modules, a successful translation from glove box-processed small-area OSCs to air-processed large-area OSC sub-modules can be realized with the lowest EPBT in comparison to other solar cell technologies and the lowest GHG emissions.

Data availability statement

The data that supports the findings of this study are properly cited with literature, and available from the corresponding author upon reasonable request.

Conflict of interest

The authors declare that the work was conducted in the absence of any commercial or financial relationships that could be construed to be a potential conflict of interest.

Author contributions

S R and J Y K conceptualized the work, wrote and edited the manuscript. All authors contributed to the literature review and discussion of the results and commented on the manuscript.

Funding

This work has been financially supported by the National Research Foundation of Korea (NRF) Grant funded by the Korea government (MSIT) (Grant No. 2021R1A2C3008724).

ORCID iDs

Shafket Rasool  <https://orcid.org/0000-0003-3240-8185>

Jin Young Kim  <https://orcid.org/0000-0002-6595-4468>

References

- [1] IEA 2021 *World Energy Outlook 2021* (Paris: IEA) (available at: www.iea.org/reports/world-energy-outlook-2021)
- [2] Chapin D M, Fuller C S and Pearson G L 1954 A new silicon p-n junction photocell for converting solar radiation into electrical power *J. Appl. Phys.* **25** 676–7
- [3] Yoshikawa K *et al* 2017 Silicon heterojunction solar cell with interdigitated back contacts for a photoconversion efficiency over 26% *Nat. Energy* **2** 17032
- [4] Rohatgi A, Zhu K, Tong J, Kim D H, Reichmanis E, Rounsaville B, Prakash V and Ok Y-W 2020 26.7% efficient 4-terminal perovskite-silicon tandem solar cell composed of a high-performance semitransparent

- perovskite cell and a doped poly-Si/SiO_x passivating contact silicon cell *IEEE J. Photovolt.* **10** 417–22
- [5] Tang C W 1986 Two-layer organic photovoltaic cell *Appl. Phys. Lett.* **48** 183–5
- [6] National Renewable Energy Laboratory. Best-research-cell-efficiencies-rev211011 (available at: www.nrel.gov/pv/cell-efficiency.html)
- [7] Zheng Z, Wang J, Bi P, Ren J, Wang Y, Yang Y, Liu X, Zhang S and Hou J 2021 Tandem organic solar cell with 20.2% efficiency *Joule* **6** 171–84
- [8] He C *et al* 2022 Asymmetric electron acceptor enables highly luminescent organic solar cells with certified efficiency over 18 *Nat. Commun.* **13** 2598
- [9] Zhu L *et al* 2022 Single-junction organic solar cells with over 19% efficiency enabled by a refined double-fibril network morphology *Nat. Mater.* **21** 656–63
- [10] Jørgensen M *et al* 2013 The state of organic solar cells—a meta analysis *Sol. Energy Mater. Sol. Cells* **119** 84–93
- [11] Zhao W, Li S, Yao H, Zhang S, Zhang Y, Yang B and Hou J 2017 Molecular optimization enables over 13% efficiency in organic solar cells *J. Am. Chem. Soc.* **139** 7148–51
- [12] Wang G, Adil M A, Zhang J and Wei Z 2018 Large-area organic solar cells: material requirements, modular designs, and printing methods *Adv. Mater.* **31** 1805089
- [13] Qin F *et al* 2021 54 cm² large-area flexible organic solar modules with efficiency above 13% *Adv. Mater. Weinheim* **33** 2103017
- [14] Kan B *et al* 2015 A series of simple oligomer-like small molecules based on oligothiophenes for solution-processed solar cells with high efficiency *J. Am. Chem. Soc.* **137** 3886–93
- [15] Fan J *et al* 2022 High-performance organic solar modules via bilayer-merged-annealing assisted blade coating *Adv. Mater.* **34** 2110569
- [16] Jiang M, Bai H R, Zhi H F, Sun J-K, Wang J-L, Zhang F and An Q 2021 Two-pronged effect of warm solution and solvent-vapor annealing for efficient and stable all-small-molecule organic solar cells *ACS Energy Lett.* **6** 2898–906
- [17] Sun K *et al* 2015 A molecular nematic liquid crystalline material for high-performance organic photovoltaics *Nat. Commun.* **6** 6013
- [18] Jae K L, Wan L M, Brabec C J, Yuen J, Moon J S, Kim J Y, Lee K, Bazan G C and Heeger A J 2008 Processing additives for improved efficiency from bulk heterojunction solar cells *J. Am. Chem. Soc.* **130** 3619–23
- [19] Kyaw A K K, Wang D H, Luo C, Cao Y, Nguyen T-Q, Bazan G C and Heeger A J 2014 Effects of solvent additives on morphology, charge generation, transport, and recombination in solution-processed small-molecule solar cells *Adv. Energy Mater.* **4** 1301469
- [20] Hoang Q V *et al* 2017 Effects of morphology evolution on solution-processed small molecule photovoltaics: via a solvent additive *J. Mater. Chem. C* **5** 7837–44
- [21] Lu L, Xu T, Chen W, Landry E S and Yu L 2014 Ternary blend polymer solar cells with enhanced power conversion efficiency *Nat. Photon.* **8** 716–22
- [22] Ma R *et al* 2022 High-efficiency ternary organic solar cells with a good figure-of-merit enabled by two low-cost donor polymers *ACS Energy Lett.* **7** 2547–56
- [23] Vohra V, Kawashima K, Kakara T, Koganezawa T, Osaka I, Takimiya K and Murata H 2015 Efficient inverted polymer solar cells employing favourable molecular orientation *Nat. Photon.* **9** 403–8
- [24] Liu Y, Zhao J, Li Z, Mu C, Ma W, Hu H, Jiang K, Lin H, Ade H and Yan H 2014 Aggregation and morphology control enables multiple cases of high-efficiency polymer solar cells *Nat. Commun.* **5** 5293
- [25] Zhao J, Li Y, Yang G, Jiang K, Lin H, Ade H, Ma W and Yan H 2016 Efficient organic solar cells processed from hydrocarbon solvents *Nat. Energy* **1** 15027
- [26] Rasool S *et al* 2019 High-efficiency non-halogenated solvent processable polymer/PCBM solar cells: via fluorination-enabled optimized nanoscale morphology *J. Mater. Chem. A* **7** 24992–5002
- [27] Guo X *et al* 2013 Polymer solar cells with enhanced fill factors *Nat. Photon.* **7** 825–33
- [28] Gong X, Tong M, Brunetti F G, Seo J, Sun Y, Moses D, Wudl F and Heeger A J 2011 Bulk heterojunction solar cells with large open-circuit voltage: electron transfer with small donor-acceptor energy offset *Adv. Mater.* **23** 2272–7
- [29] Proctor C M, Kuik M and Nguyen T Q 2013 Charge carrier recombination in organic solar cells *Prog. Polym. Sci.* **38** 1941–60
- [30] Ma W, Tumbleston J R, Wang M, Gann E, Huang F and Ade H 2013 Domain purity, miscibility, and molecular orientation at donor/acceptor interfaces in high performance organic solar cells: paths to further improvement *Adv. Energy Mater.* **3** 864–72
- [31] Tumbleston J R, Collins B A, Yang L, Stuart A C, Gann E, Ma W, You W and Ade H 2014 The influence of molecular orientation on organic bulk heterojunction solar cells *Nature Photon.* **8** 385–91
- [32] Yuan J *et al* 2019 Single-junction organic solar cell with over 15% efficiency using fused-ring acceptor with electron-deficient core single-junction organic solar cell with over 15% efficiency using fused-ring acceptor with electron-deficient core *Joule* **3** 1140–51
- [33] Yu H *et al* 2020 Tailoring non-fullerene acceptors using selenium-incorporated heterocycles for organic solar cells with over 16% efficiency *J. Mater. Chem. A* **8** 23756–65
- [34] Wang H *et al* 2022 Chlorination enabling a low-cost benzodithiophene-based wide-bandgap donor polymer with an efficiency of over 17% *Adv. Mater.* **34** 2105483
- [35] Liu Q *et al* 2020 18% efficiency organic solar cells *Sci. Bull.* **65** 272–5
- [36] Wang J *et al* 2022 A new polymer donor enables binary all-polymer organic photovoltaic cells with 18% efficiency and excellent mechanical robustness *Adv. Mater.* **34** 2205009
- [37] Sun C, Pan F, Bin H, Zhang J, Xue L, Qiu B, Wei Z, Zhang Z-G and Li Y 2018 A low cost and high performance polymer donor material for polymer solar cells *Nat. Commun.* **9** 743
- [38] Li C *et al* 2021 Non-fullerene acceptors with branched side chains and improved molecular packing to exceed 18% efficiency in organic solar cells *Nat. Energy* **6** 605–13
- [39] Abbas Z, Un S, Haris M, Song C E, Lee H K, Lee S K, Shin W S, Park T and Lee J-C 2022 Nano energy optimized vertical phase separation via systematic Y6 inner side-chain modulation for non-halogen solvent processed inverted organic solar cells *Nano Energy* **101** 107574
- [40] Cui Y *et al* 2019 Over 16% efficiency organic photovoltaic cells enabled by a chlorinated acceptor with increased open-circuit voltages *Nat. Commun.* **10** 2515
- [41] He Q, Ufimkin P, Anié F, Hu X, Kafourou P, Rimmele M, Rapley C L and Ding B 2022 Molecular engineering of Y-series acceptors for nonfullerene organic solar cells *SusMat* **2** 591–606
- [42] Chai G *et al* 2021 Fine-tuning of side-chain orientations on nonfullerene acceptors enables organic solar cells with 17.7% efficiency *Energy Environ. Sci.* **14** 3469–79
- [43] Liu G, Xia R, Huang Q, Zhang K, Hu Z, Jia T, Liu X, Yip H-L and Huang F 2021 Tandem organic solar cells with 18.7% efficiency enabled by suppressing the charge

- recombination in front sub-cell *Adv. Funct. Mater.* **31** 2103283
- [44] Wang J, Zheng Z, Zu Y, Wang Y, Liu X, Zhang S, Zhang M and Hou J 2021 A tandem organic photovoltaic cell with 19.6% efficiency enabled by light distribution control *Adv. Mater.* **33** 2102787
- [45] Holliday S *et al* 2016 High-efficiency and air-stable P3HT-based polymer solar cells with a new non-fullerene acceptor *Nat. Commun.* **7** 11585
- [46] Qi F *et al* 2021 Over 17% efficiency binary organic solar cells with photoresponses reaching 1000 nm enabled by selenophene-fused nonfullerene acceptors *ACS Energy Lett.* **6** 9–15
- [47] Chang Y 2021 Achieving efficient ternary organic solar cells using structurally similar non-fullerene acceptors with varying flanking side chains *ACS Energy Mater.* **11** 2100079
- [48] Chen H *et al* 2021 A guest-assisted molecular-organization approach for >17% efficiency organic solar cells using environmentally friendly solvents *Nat. Energy* **6** 1045–53
- [49] Li Y, Cai Y, Xie Y, Song J, Wu H, Tang Z, Zhang J, Huang F and Sun Y 2021 A facile strategy for third-component selection in non-fullerene acceptor-based ternary organic solar cells *Energy Environ. Sci.* **14** 5009–16
- [50] Lin Y *et al* 2022 18.9% efficient organic solar cells based on n-doped bulk-heterojunction and halogen-substituted self-assembled monolayers as hole extracting interlayers *Adv. Energy Mater.* **12** 2202503
- [51] Wang J *et al* 2022 An asymmetric wide-bandgap acceptor simultaneously enabling highly efficient single-junction and tandem organic solar cells *Energy Environ. Sci.* **15** 1585–93
- [52] Rasool S, Van V D, Song C E, Lee H K, Lee S K, Lee J-C, Moon S-J and Shin W S 2019 Room temperature processed highly efficient large-area polymer solar cells achieved with molecular engineering of copolymers *Adv. Energy Mater.* **9** 1900168
- [53] Zhang B, Yang F, Chen S, Chen H, Zeng G, Shen Y, Li Y and Li Y 2022 Fluid mechanics inspired sequential blade-coating for high-performance large-area organic solar modules *Adv. Funct. Mater.* **32** 2202011
- [54] Cho Y *et al* 2023 CF₃-terminated side chain enables efficiencies surpassing 18.2% and 16.1% in small- and large-scale manufacturing of organic solar cells *ACS Energy Lett.* **8** 96–106
- [55] Badgujar S, Lee G Y, Park T, Song C E, Park S, Oh S, Shin W S, Moon S-J, Lee J-C and Lee S K 2016 High-performance small molecule via tailoring intermolecular interactions and its application in large-area organic photovoltaic modules *Adv. Energy Mater.* **6** 1600228
- [56] Yuan J *et al* 2021 Patterned blade coating strategy enables the enhanced device reproducibility and optimized morphology of organic solar cells *Adv. Energy Mater.* **11** 2100098
- [57] Dong S, Jia T, Zhang K, Jing J and Huang F 2020 Single-component non-halogen solvent-processed high-performance organic solar cell module with efficiency over 14% *Joule* **4** 2004–16
- [58] Chaturvedi N, Gasparini N, Corzo D, Bertrandie J, Wehbe N, Troughton J and Baran D 2021 All slot-die coated non-fullerene organic solar cells with PCE 11% *Adv. Funct. Mater.* **31** 2009996
- [59] Polymer F, Diodes L-E, Polymer C, Higuchi H, Yoshioka M and Nagatsuka T 2002 High-performance, flexible polymer light-emitting diodes fabricated by a continuous polymer coating process *Adv. Mater.* **14** 915–8
- [60] Khim D, Han H, Baeg K J, Kim J, Kwak S-W, Kim D-Y and Noh Y-Y 2013 Simple bar-coating process for large-area, high-performance organic field-effect transistors and ambipolar complementary integrated circuits *Adv. Mater. Weinheim* **25** 4302–8
- [61] Han Y W, Lee H S and Moon D K 2021 Printable and semitransparent nonfullerene organic solar modules over 30 cm²: introducing an energy-level controllable hole transport layer *ACS Appl. Mater. Interfaces* **13** 19085–98
- [62] Jeong J H, Jahandar M, Prasetyo A, Kim J M, Kim J H, Kim S and Lim D C 2021 Multi-dimensional interfacial engineering for a practical large-area transparent flexible organic photovoltaics *Chem. Eng. J.* **419** 129672
- [63] Jahandar M, Prasetyo A, Lee C, Kim H, Kim A R, Heo J, Kim Y, Kim S and Lim D C 2022 Highly efficient flexible organic photovoltaic modules for sustainable energy harvesting under low-light condition via suppressing voltage-drop by metal-mediated cross-linkable polymer interfacial layer *Chem. Eng. J.* **448** 137555
- [64] Roth B, Søndergaard R R and Krebs F C 2014 Roll-to-roll printing and coating techniques for manufacturing large-area flexible organic electronics (Elsevier Ltd) (<https://doi.org/10.1016/B978-1-78242-035-4.00007-5>)
- [65] Zhang Y *et al* 2021 Graded bulk-heterojunction enables 17% binary organic solar cells via nonhalogenated open air coating *Nat. Commun.* **12** 4815
- [66] Yoon S *et al* 2022 High-performance scalable organic photovoltaics with high thickness tolerance from 1 cm² to above 50 cm² *Joule* **6** 1–17
- [67] Liao C Y *et al* 2020 Processing strategies for an organic photovoltaic module with over 10% efficiency *Joule* **4** 189–206
- [68] Lee T, Oh S, Rasool S, Song C E, Kim D, Lee S K, Shin W S and Lim E 2020 Non-halogenated solvent-processed ternary-blend solar cells via alkyl-side-chain engineering of a non-fullerene acceptor and their application in large-area devices *J. Mater. Chem. A* **8** 10318–30
- [69] Kim H S, Rasool S, Shin W S, Song C E and Hwang D-H 2020 Alkylated indacenodithiophene-based non-fullerene acceptors with extended π -conjugation for high-performance large-area organic solar cells *ACS Appl. Mater. Interfaces* **12** 50638–47
- [70] Park S H, Park S, Lee S, Kim J, Ahn H, Kim B J, Chae B and Son H J 2020 Development of highly efficient large area organic photovoltaic module: effects of nonfullerene acceptor *Nano Energy* **77** 105147
- [71] Zhang L, Zhao H, Lin B, Yuan J, Xu X, Wu J, Zhou K, Guo X, Zhang M and Ma W 2019 A blade-coated highly efficient thick active layer for non-fullerene organic solar cells *J. Mater. Chem. A* **7** 22265–73
- [72] Sun R *et al* 2020 A layer-by-layer architecture for printable organic solar cells overcoming the scaling lag of module efficiency *Joule* **4** 407–19
- [73] Dong X, Jiang Y, Sun L, Qin F, Zhou X, Lu X, Wang W and Zhou Y 2022 Large-area organic solar modules with efficiency over 14% *Adv. Funct. Mater.* **32** 2110209
- [74] Zeng G *et al* 2022 Realizing 17.5% efficiency flexible organic solar cells via atomic-level chemical welding of silver nanowire electrodes *J. Am. Chem. Soc.* **144** 8658–68
- [75] Chen X, Xu G, Zeng G, Gu H, Chen H, Xu H, Yao H, Li Y, Hou J and Li Y 2020 Realizing ultrahigh mechanical flexibility and >15% efficiency of flexible organic solar cells via a “welding” flexible transparent electrode *Adv. Mater.* **32** 1908478
- [76] Chen Y, Wan J, Xu G, Wu X, Li X, Shen Y, Yang F, Ou X, Li Y and Li Y 2022 “Reinforced concrete”-like flexible transparent electrode for organic solar cells with high efficiency and mechanical robustness *Sci. China Chem.* **65** 1164–72
- [77] Pokuri B S S, Sit J, Wodo O, Baran D, Ameri T, Brabec C J, Moule A J and Ganapathysubramanian B 2017 Nanoscale

- morphology of doctor bladed versus spin-coated organic photovoltaic films *Adv. Energy Mater.* **7** 1701269
- [78] Li H, Liu S, Wu X, Qi Q, Zhang H, Meng X, Hu X, Ye L and Chen Y 2022 A general enlarging shear impulse approach to green printing large-area and efficient organic photovoltaics *Energy Environ. Sci.* **15** 2130–8
- [79] Zhao H *et al* 2020 Hot hydrocarbon-solvent slot-die coating enables high-efficiency organic solar cells with temperature-dependent aggregation behavior *Adv. Mater.* **32** 2002302
- [80] Weng K, Ye L, Zhu L, Xu J, Zhou J, Feng X, Lu G, Tan S, Liu F and Sun Y 2020 Optimized active layer morphology toward efficient and polymer batch insensitive organic solar cells *Nat. Commun.* **11** 2855
- [81] Liu S *et al* 2020 Printable and large-area organic solar cells enabled by a ternary pseudo-planar heterojunction strategy *Adv. Funct. Mater.* **30** 2003223
- [82] Jee M H, Ryu H S, Lee D, Lee W and Woo H Y 2022 Recent advances in nonfullerene acceptor-based layer-by-layer organic solar cells using a solution process *Adv. Sci.* **9** 2201876
- [83] Khenkin M V *et al* 2020 reporting for perovskite photovoltaics based on *Nat. Energy* **5** 35–49
- [84] Reese M O *et al* 2011 Consensus stability testing protocols for organic photovoltaic materials and devices *Sol. Energy Mater. Sol. Cells* **95** 1253–67
- [85] Mateker W R and McGehee M D 2017 Progress in understanding degradation mechanisms and improving stability in organic photovoltaics *Adv. Mater.* **29** 1603940
- [86] Xu X, Li D, Yuan J, Zhou Y and Zou Y 2021 EnergyChem recent advances in stability of organic solar cells *Energy Chem.* **3** 100046
- [87] Cros S, de Bettignies R, Berson S, Bailly S, Maisse P, Lemaitre N and Guillerez S 2011 Definition of encapsulation barrier requirements: a method applied to organic solar cells *Sol. Energy Mater. Sol. Cells* **95** S65–9
- [88] Angmo D and Krebs F C 2015 Over 2years of outdoor operational and storage stability of ITO-free, fully roll-to-roll fabricated polymer solar cell modules *Energy Technol.* **3** 774–83
- [89] Castro-Hermosa S, Top M, Dagar J, Fahlteich J and Brown T M 2019 Quantifying performance of permeation barrier—encapsulation systems for flexible and glass-based electronics and their application to perovskite solar cells *Adv. Electron. Mater.* **5** 1800978
- [90] Zhang J, Tan H S, Guo X, Facchetti A and Yan H 2018 Material insights and challenges for non-fullerene organic solar cells based on small molecular acceptors *Nat. Energy* **3** 720–31
- [91] Fraga Domínguez I, Distler A and Lüer L 2017 Stability of organic solar cells: the influence of nanostructured carbon materials *Adv. Energy Mater.* **7** 1601320
- [92] Conings B, Bertho S, Vandewal K, Senes A, D'Haen J, Manca J and Janssen R A J 2010 Modeling the temperature induced degradation kinetics of the short circuit current in organic bulk heterojunction solar cells *Appl. Phys. Lett.* **96** 32–35
- [93] Liu Q, Toudert J, Liu F, Mantilla-Perez P, Bajo M M, Russell T P and Martorell J 2017 Circumventing UV light induced nanomorphology disorder to achieve long lifetime PTB7-Th:PCBM based solar cells *Adv. Energy Mater.* **7** 1701201
- [94] Rasool S, van Doan V, Lee H K, Lee S K, Lee J-C, Moon S-J, So W W, Song C E and Shin W S 2019 Enhanced photostability in polymer solar cells achieved with modified electron transport layer *Thin Solid Films* **669** 42–48
- [95] Cheng P, Yan C, Lau T K, Mai J, Lu X and Zhan X 2016 Molecular lock: a versatile key to enhance efficiency and stability of organic solar cells *Adv. Mater.* **28** 5822–9
- [96] Wu S-C, Strover L T, Yao X, Chen X-Q, Xiao W-J, Liu L-N, Wang J, Visoly-Fisher I, Katz E A and Li W-S 2018 UV-cross-linkable donor–acceptor polymers bearing a photostable conjugated backbone for efficient and stable organic photovoltaics *ACS Appl. Mater. Interfaces* **10** 35430–40
- [97] Zhu Y, Gadisa A, Peng Z, Ghasemi M, Ye L, Xu Z, Zhao S and Ade H 2019 Rational strategy to stabilize an unstable high-efficiency binary nonfullerene organic solar cells with a third component *Adv. Energy Mater.* **9** 1900376
- [98] Liu B *et al* 2023 Efficient and stable organic solar cells enabled by multicomponent photoactive layer based on one-pot polymerization *Nat. Commun.* **14** 967
- [99] Chang Y M, Liao C Y, Lee C C, Lin S-Y, Teng N-W and Hwei-Shuan Tan P 2019 All solution and ambient processable organic photovoltaic modules fabricated by slot-die coating and achieved a certified 7.56% power conversion efficiency *Sol. Energy Mater. Sol. Cells* **202** 110064
- [100] Li S, Fu Q, Meng L, Wan X, Ding L, Lu G, Lu G, Yao Z, Li C and Chen Y 2022 Achieving over 18% efficiency organic solar cell enabled by a ZnO-based hybrid electron transport layer with an operational lifetime up to 5 years *Angew. Chem., Int. Ed.* **61** e202207397
- [101] Dahlström S, Wilken S, Zhang Y, Ahläng C, Barlow S, Nyman M, Marder S R and Österbacka R 2021 Cross-linking of doped organic semiconductor interlayers for organic solar cells: potential and challenges *ACS Appl. Energy Mater.* **4** 14458–66
- [102] Leccisi E and Fthenakis V 2021 Life cycle energy demand and carbon emissions of scalable single-junction and tandem perovskite PV *Prog. Photovolt., Res. Appl.* **29** 1078–92
- [103] Tian X, Stranks S D and You F 2021 Life cycle assessment of recycling strategies for perovskite photovoltaic modules *Nat. Sustain.* **4** 821–9
- [104] Riede M, Spoltore D and Leo K 2021 Organic solar cells—the path to commercial success *Adv. Energy Mater.* **11** 2002653
- [105] Li Q, Monticelli C and Zanelli A 2022 Life cycle assessment of organic solar cells and perovskite solar cells with graphene transparent electrodes *Renew. Energy* **195** 906–17